Rational Design of Metal-Free Nitrogen-Doped Carbon for Controllable Reduction of CO_2 to Syngas

Guangbin An [1], Kang Wang [1], Min Yang [2], Jiye Zhang [3], Haijian Zhong [2,*], Liang Wang [1] and Huazhang Guo [1,*]

[1] Institute of Nanochemistry and Nanobiology, School of Environmental and Chemical Engineering, Shanghai University, 99 Shangda Road, Shanghai 200444, China
[2] School of Information Engineering, Gannan Medical University, Ganzhou 341000, China
[3] School of Materials Science and Engineering, Shanghai University, 99 Shangda Road, Shanghai 200444, China
* Correspondence: hjzhong2007@gmu.edu.cn (H.Z.); guohuazhang@shu.edu.cn (H.G.)

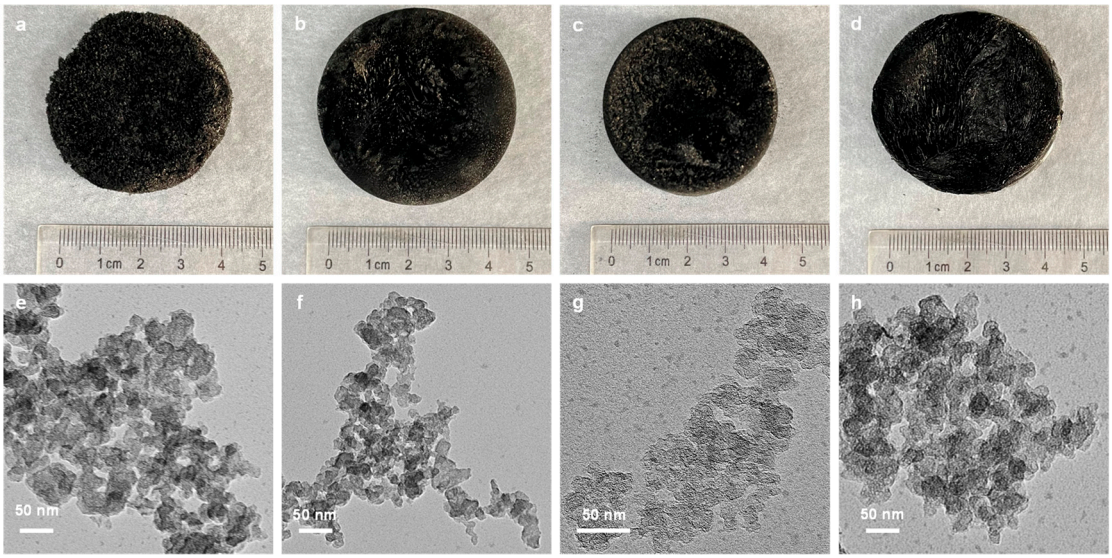


Figure S1. (**a**), (**b**), (**c**) and (**d**) Pictures of p-NCB1, p-NCB2, p-NCB3 and p-NCB4. (**e**), (**f**), (**g**) and (**h**) TEM images of NCB1, NCB2, NCB3 and NCB4.

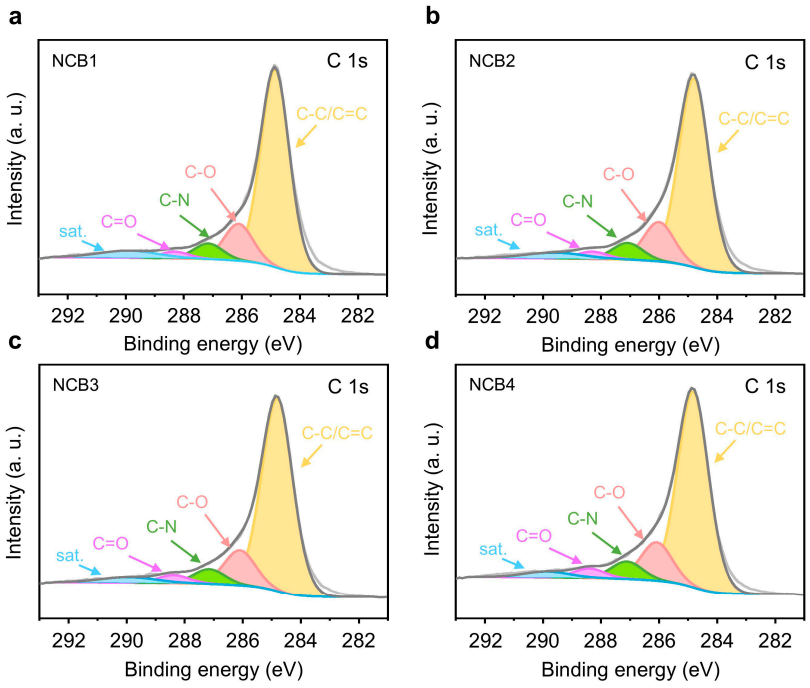


Figure S2. The high-resolution C 1s XPS spectra of NCB1 (**a**), NCB2 (**b**), NCB3 (**c**) and NCB4 (**d**).

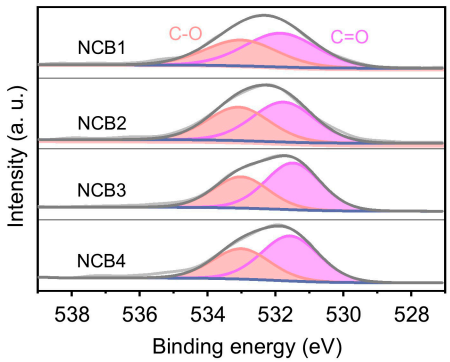


Figure S3. (**a**), (**b**), (**c**) and (**d**) The high-resolution O 1s XPS spectra of NCB1, NCB2, NCB3 and NCB4.

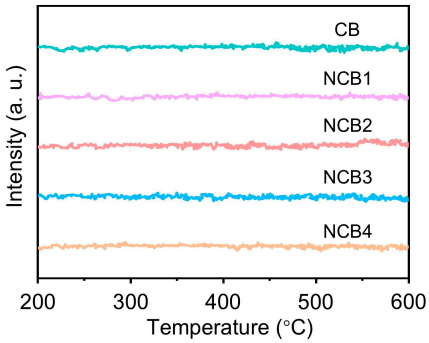


Figure S4. NH_3-TPD of CB, NCB1, NCB2, NCB3 and NCB4.

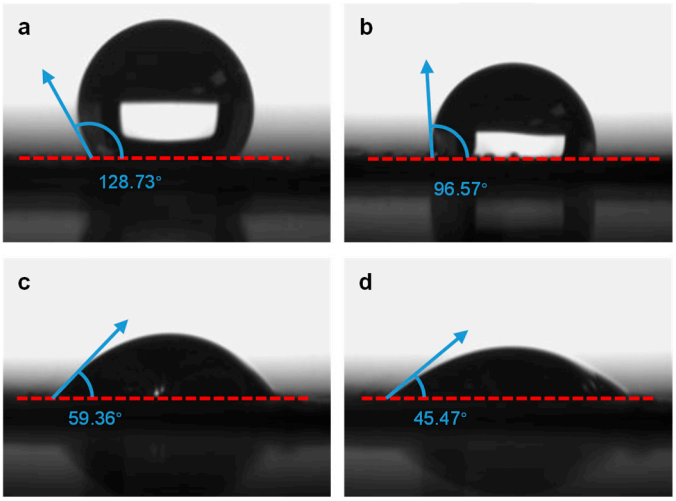


Figure S5. Contact angle of (**a**) NCB1, (b) NCB2, (c) NCB3 and (d) NCB4.

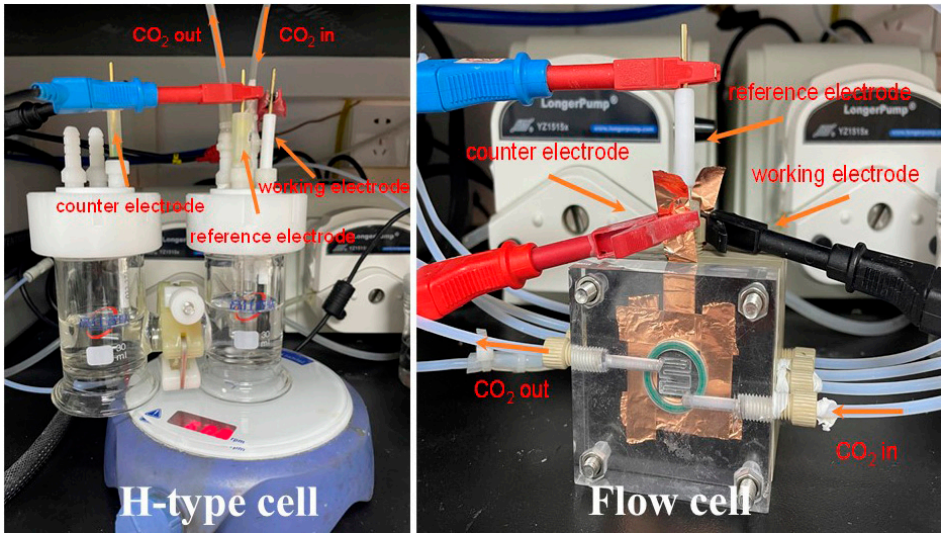


Figure S6. The physical picture of H-type cell and flow cell.

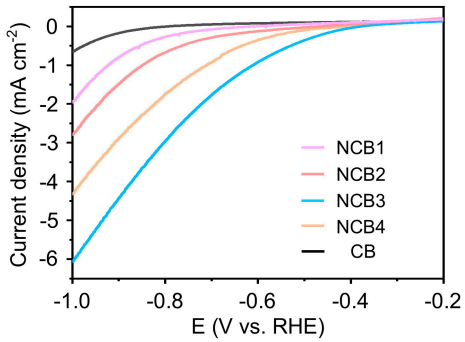


Figure S7. LSV curves of NCB1, NCB2, NCB3, NCB4 and CB in CO_2-saturated 0.1 M $KHCO_3$ solution.

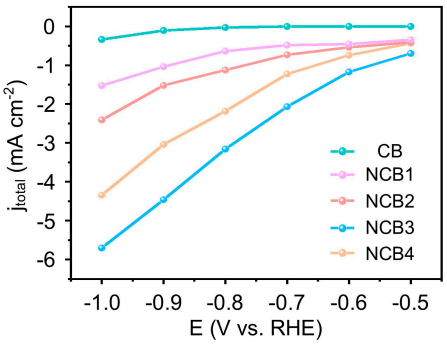


Figure S8. Total current density of CB, NCB1, NCB2, NCB3 and NCB4 at different electrolytic potentials in H-type cell.

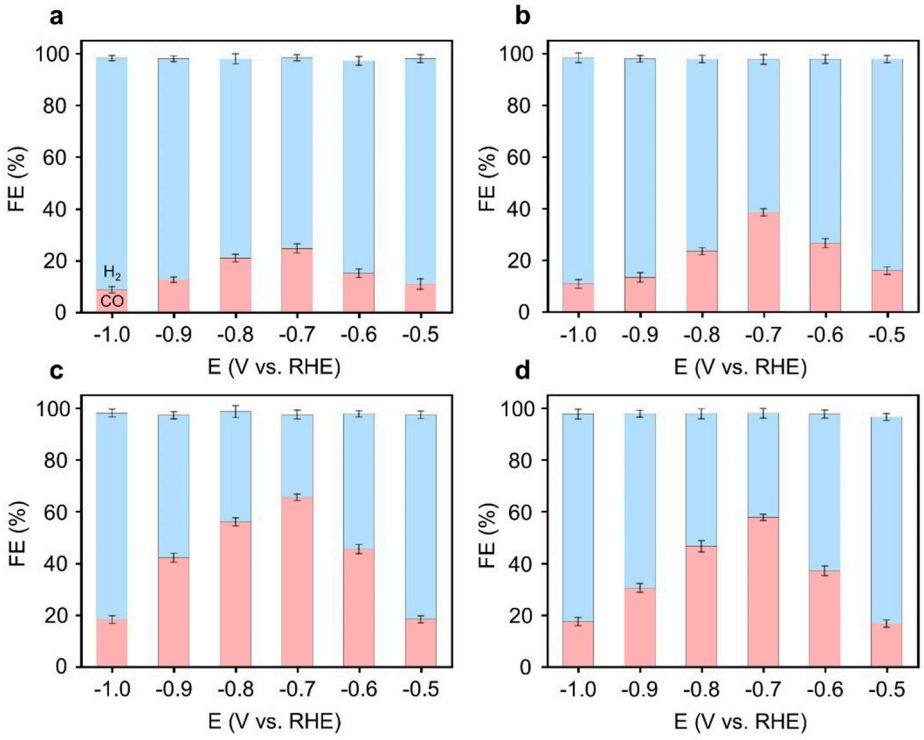


Figure S9. Faradaic efficiency of H_2 and CO in a H-type cell on the various catalysts at different potentials in CO_2-satureted 0.1 M $KHCO_3$ solution. (**a**) NCB1, (**b**) NCB2, (**c**) NCB3 and (**d**) NCB4.

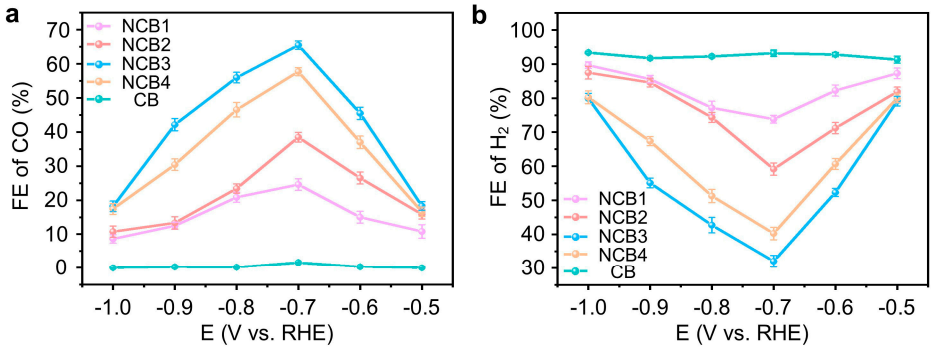


Figure S10. (**a**) CO and (b) H_2 FE of NCB1, NCB2, NCB3, NCB4 and CB.

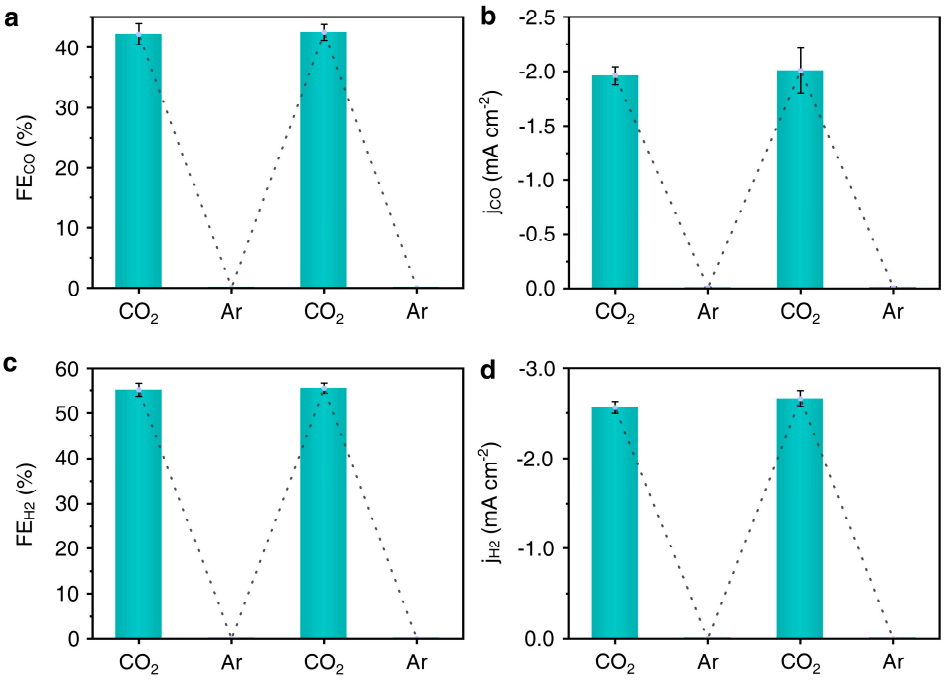


Figure S11. (**a**) FE_{CO} and (**b**) j_{CO} for NCB3 when alternatively, supplying CO_2 and Ar feedstocks at -0.9 V vs. RHE. (**c**) FE_{H2} and (**d**) j_{H2} for NCB3 when alternatively supplying CO_2 and Ar feedstocks at -0.9 V vs. RHE.

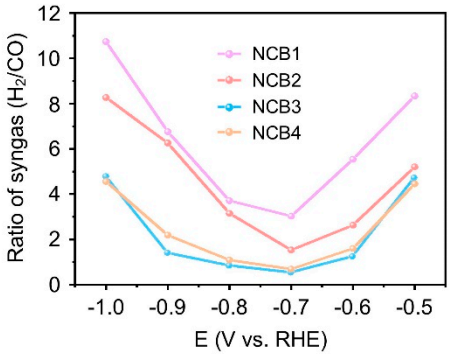


Figure S12. The ratio of syngas at different potentials in H-type cell.

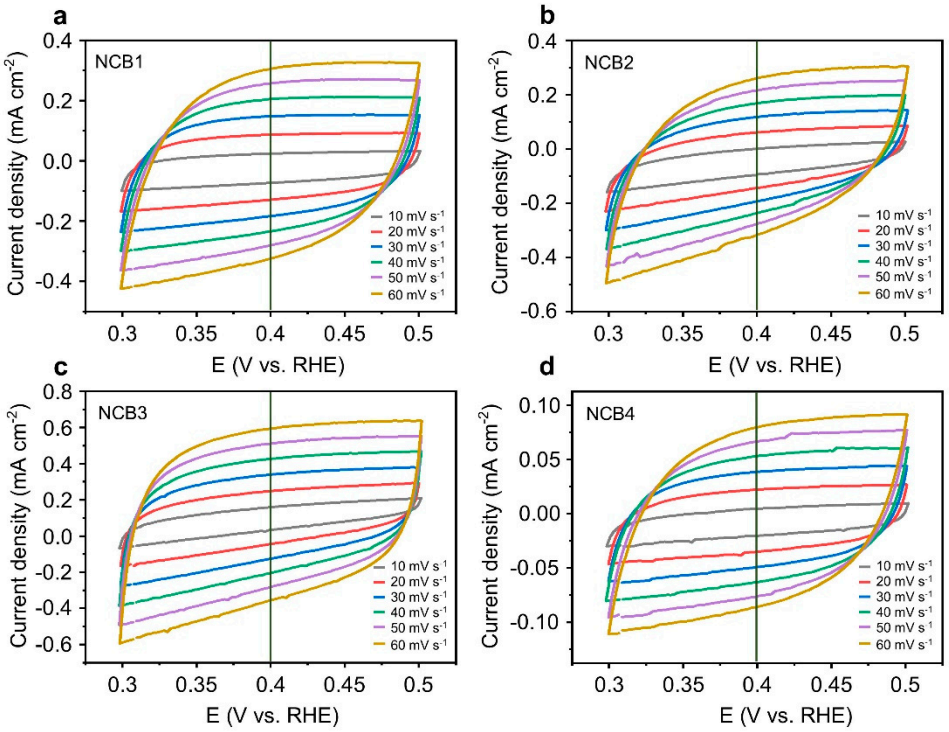


Figure S13. CV curves of various catalysts studied in 0.1 M $KHCO_3$ at different scan rates (10, 20, 30,40, 50 and 60 mV s^{-1}) for estimation of double layer capacitance. (**a**) NCB1, (**b**) NCB2, (**c**) NCB3 and (**d**) NCB4.

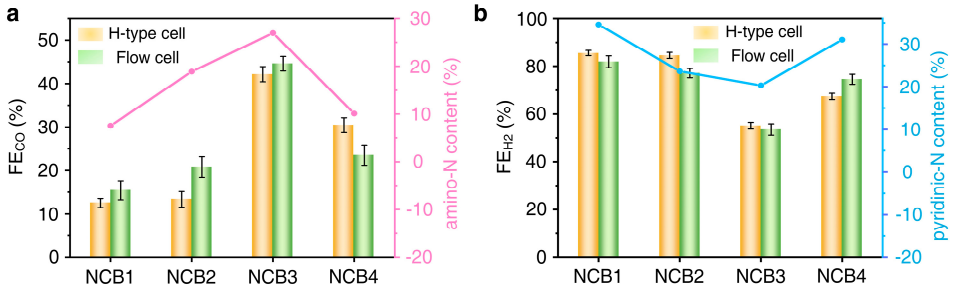


Figure S14. The relationship between amino-N (a) and pyridinic-N (b) content of NCB3 and FE_{CO} and FE_{H2} in a H-type cell and flow cell, respectively.

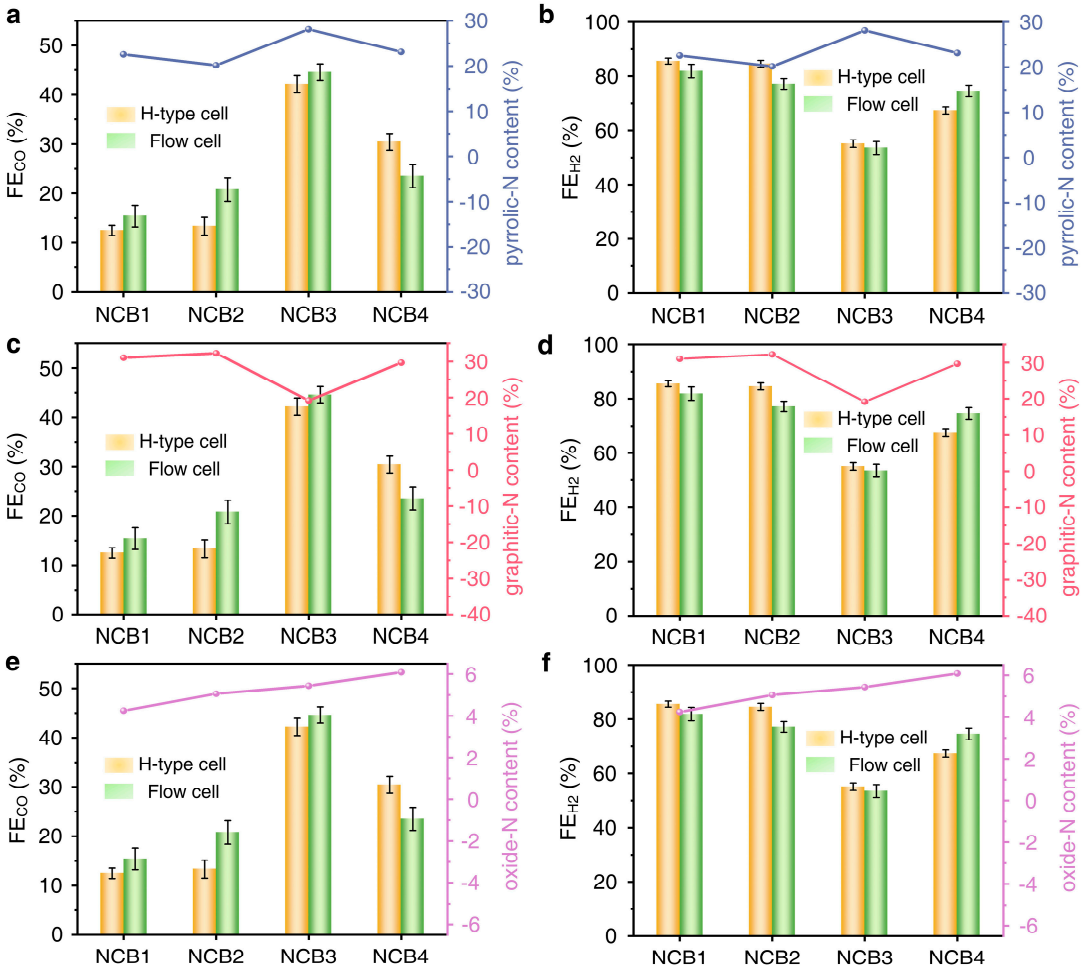


Figure S15. The relationship between the content of pyrrolic-N (a-b), graphitic-N (c-d), and oxide-N (e-f) and FE_{CO} and FE_{H2} in H-type cell and flow cell, respectively.

Table S1. Weight of various sample before and after calcination.

Samples	Before calcination (g)	After calcination (g)	Yield (%)
NCB1	0.285	0.152	53.33
NCB2	0.488	0.203	41.60
NCB3	0.715	0.532	74.41
NCB4	0.885	0.619	69.94

Table S2. C, N and O contents of various samples (data from XPS analysis).

Samples	C (at.%)	N (at.%)	O (at.%)
CB	97.04	-	2.96
NCB1	91.21	3.14	5.65
NCB2	92.46	3.18	4.36
NCB3	90.99	4.28	4.73
NCB4	89.05	5.28	5.67

Table S3. C-C/C=C, C-O, C-N and C=O groups contents of various samples (data from XPS analysis).

Samples	C-C/C=C (at.%)	C-O (at.%)	C-N (at.%)	C=O (at.%)
NCB1	76.89	14.34	6.14	2.63
NCB2	74.83	15.58	6.68	2.91
NCB3	76.78	14.04	5.92	3.26
NCB4	74.88	14.74	6.73	3.62

Table S4. C=O and C-O groups contents of various samples (data from XPS analysis).

Samples	C=O (at.%)	C-O (at.%)
NCB1	56.59	43.41
NCB2	54.40	45.60
NCB3	59.88	40.12
NCB4	59.70	40.30

Table S5. Pyridinic-N, amino-N, pyrrolic-N, graphitic-N and oxide-N contents of various samples.

Samples	pyridinic-N (at.%)	amino-N (at.%)	pyrrolic-N (at.%)	graphitic-N (at.%)	oxide-N (at.%)
NCB1	34.58	7.55	22.58	31.04	4.25
NCB2	23.63	18.88	20.17	32.26	5.06
NCB3	20.30	26.94	28.12	19.20	5.44
NCB4	31.02	10.11	23.12	29.66	6.09

Table S6. The results of N_2 adsorption-desorption for different samples.

Samples	S_{BET} (m^2 g^{-1}) [a]	V_{Total} (cm^3 g^{-1}) [b]	$\bar{D}$ (nm) [c]
CB	138.24	0.082	2.37
NCB1	268.94	0.24	3.57
NCB2	458.29	0.66	5.76
NCB3	602.71	0.86	5.71
NCB4	582.70	0.80	5.49

[a] S_{BET} (BET surface area) is calculated by BET method. [b] V_{Total} (Total pore volume) is the single point adsorption at P/P_0=0.99. [c] $\bar{D}$ (average pore diameter) is calculated by BJH method.

Table S7. Performance comparison of catalysts for syngas formation.

Catalysts	FE_{CO} (%)	CO/H_2 ratios	current density (mA/cm^2)	applied potentials (V_{RHE})	Ref.
NCB3	64.14	0.52-4.77	1.9	-0.5-1.0 V	This work
OA-PCN	40	0.67	-7	-0.56-0.86 V	1
Pd/C	62	0.5	1.5	-0.5-0.8 V	2
MPC-1000	62	not reported	-6	-0.3-0.7 V	3
Pd/PdOx	58	1.45	11	0.55-0.9 V	4
$Cu_{14}Zn_{86}O$/CNT	not reported	1	1.5	-0.5-0.88 V	5
Ni-NG	53	1.10	12.4	-0.5-0.9 V	6
Co@CoNC-900	42	1	-2.7-7.9	-0.6 -0.8 V	7

Table S8. Electrical conductivity of the synthesized catalysts by the 4-point probe method under a pressure of 10 MPa.

Samples	NCB1	NCB2	NCB3	NCB4
electrical resistivity (mΩ cm)	239.5	149.3	70.1	84.3
conductivity $\times 10^3$ (S cm^{-1})	4.2	6.7	14.3	11.8

References

1. Meng, N.; Zhou, W.; Yu, Y.; Liu Y.; Zhang, B. Superficial hydroxyl and amino groups synergistically active polymeric carbon nitride for CO_2 electro-reduction. *ACS Catal.* **2019**, *9*, 10983-10989.
2. Sheng, W.; Kattel, S.; Yao, S.; Yan, B.; Liang, Z.; Hawxhurst, C.; Wu, Q.; Chen, J. G. Electrochemical reduction of CO_2 to synthesis gas with controlled CO/H_2 ratios. *Energy Environ. Sci.* **2017**. *10*, 1180-1185.
3. Pan, F.; Liang, A.; Duan, Y.; Liu, Q.; Zhang J.; Li, Y. Self-growth templating synthesis of 3D N,P, co-doped mesoporous carbon frameworks for efficient bifunctional oxygen and carbon dioxide electroreduction. *J. Mater. Chem. A* **2017**, *5*, 13104-13111.
4. Lu, H.; Zhang, L.; Zhong, J. H.; Yang, H.G. Partially oxidized palladium nanodots for enhanced electrocatalytic carbon dioxide reduction. *Chem.-Asian J.* **2018**, *13*, 2800-2804.
5. Hjorth, I.; Nord, M.; Rønning, M.; Yang, J.; Chen, D. Electrochemical reduction of CO_2 to synthesis gas on CNT supported $Cu_xZn_{1-x}O$ Catalysts. *Catal. Today* **2020**, 357, 311-321.

6. Jiang, K.; Siahrostami, S.; Zheng, T.; Hu, Y.; Hwang, S.; Stavitski, E.; Peng, Y.; Dynes, J.; Gangisetty, M.; Su, D.; Attenkofer, K.; Wang. H. Isolated Ni single atoms in graphene nanosheets for high-performance CO_2 reduction. *Energy Environ. Sci.* **2018**, *11*, 893-903.
7. Daiyan, R.; Chen, R.; Kumar, P.; Bedford, N.M.; Qu, J.; Cairney, J.M.; Lu, X.; Amal. R. Tuneable syngas production through CO_2 electroreduction on cobalt-carbon composite electrocatalyst. *ACS Appl. Mater. Interfaces* **2020**, *12*, 9307-9315.